



Simulation study on acoustic streaming and convective cooling in blood vessels during a high-intensity focused ultrasound thermal ablation

Maxim A. Solovchuk^a, Tony W.H. Sheu^{a,b,*}, Win-Li Lin^c, Ihyuan Kuo^d, Marc Thiriet^e

^a Department of Engineering Science and Ocean Engineering, National Taiwan University, No. 1, Section 4, Roosevelt Road, Taipei 10617, Taiwan, ROC

^b Taida Institute of Mathematical Science (TIMS), National Taiwan University, Taiwan, ROC

^c Institute of Biomedical Engineering, National Taiwan University, Taiwan, ROC

^d Medical Engineering Research Division, National Health Research Institute, Miaoli, Taiwan, ROC

^e LJLL, University of Paris # 6, Paris, France

ARTICLE INFO

Article history:

Received 22 April 2011

Received in revised form 2 September 2011

Accepted 2 September 2011

Available online 10 November 2011

Keywords:

Acoustics-thermal-fluid coupling

HIFU

Navier–Stokes equations

Acoustic streaming

Liver tumor

ABSTRACT

This study investigates the influence of blood vessels on temperature distribution during high-intensity focused ultrasound (HIFU) ablation of liver tumors. A three-dimensional acoustics-thermal-fluid coupling model is simulated to compute the temperature field in the hepatic cancerous region. The model is based on the linear Westervelt and bioheat equations as well as the non-linear Navier–Stokes equations for the liver parenchyma and blood vessels. The effect of acoustic streaming is also taken into account in the present HIFU simulation study. We found from this three-dimensional coupling study that in large blood vessel both the convective cooling and acoustic streaming can significantly change the temperature field and thermal lesion near blood vessels.

© 2011 Elsevier Ltd. All rights reserved.

1. Introduction

Human liver is a highly perfused organ, which has functions to secrete bile, store glycogen, distribute nutrients from the blood and gastrointestinal tract [1]. In addition, it eliminates endogenous/exogenous substrates and toxins. This physiologically complex and important organ is unfortunately susceptible to the primary and metastatic malignant proliferations. Hepatocellular carcinoma (HCC) is rapidly becoming the most common malignancy worldwide. The survival rate of surgical resection, while being considered as a real hope for the treatment, is only 25–30% in 5 years [2]. A high risk of postoperative recurrence is often reported for multi-focal malignancies. After repeated resections a poor success rate is expected.

HIFU therapy has been applied to ablate solid tumors in different areas of our body, including the pancreas, liver, prostate, breast, uterine fibroids, and soft-tissue sarcomas [2,3]. In comparison with the conventional tumor/cancer treatment modalities, such as the open surgery, radio- and chemo-therapy, HIFU outperforms them because of its non-invasion, non-ionization, and

comparatively fewer complications after treatment. However, lethal complications may develop if the vital blood vessels adjacent to the tumors are severely damaged. Large blood vessels are probably less vulnerable to HIFU damage than the solid tissues (such as tumor tissues) due to energy dissipation in the blood flow. Therefore, HIFU is a relatively safe alternative to ablate the tumors in close proximity to major blood vessels, where surgical resection may be hazardous.

Clinical trials have been recently conducted to evaluate the safety and effectiveness of applying the high-intensity focused ultrasound treatment of the hepatocarcinoma (HCC) [4,5]. When the liver tumor is very close to large blood vessels, surgical treatment becomes complicated. Quite recently [6] it was first shown that HIFU can safely achieve a virtually complete necrosis of tumors close to major blood vessels. After a single session of HIFU treatment, the rate of complete necrosis was about 50%. While substantial, this rate of necrosis following the HIFU ablation is not completely satisfactory. Lack of a complete response can be explained as a consequence of large tumor size and cooling effects in large vessels.

Cooling from a large blood vessel may alter the treatment efficiency. A basic understanding of the factors that can affect the tissue necrosis volume is necessary to improve the thermoablative therapy. In the past, temperature elevation in soft tissues was mostly modeled by the diffusion-type Pennes bioheat transfer equation, which has the heat source produced by the incident

* Corresponding author at: Department of Engineering Science and Ocean Engineering, National Taiwan University, No. 1, Section 4, Roosevelt Road, Taipei 10617, Taiwan, ROC. Fax: +886 2 23929885.

E-mail addresses: solovchuk@gmail.com (M.A. Solovchuk), twshsheu@ntu.edu.tw (T.W.H. Sheu).

Nomenclature

c_0	speed of ultrasound in tissue, m/s
c	specific heat, J/kg °C
\mathbf{F}	force vector per unit volume, N/m ³
k	wave number
k_t	thermal conductivity of tissue, W/m °C
I	sound intensity, W/m ²
p	acoustic pressure, N/m ²
\mathbf{P}	fluid static pressure, N/m ²
q	ultrasound power deposition, W/m ³
t	time, s
t_0	initial time, s
t_{final}	final time, s
T	temperature, °C
u	blood flow velocity, m/s
w	velocity in z direction, m/s
w_b	blood perfusion rate, kg/m ³ s
x	coordinate in the x direction

y	coordinate in the y direction
z	coordinate in the z direction

Greek symbols

α	absorption coefficient, Np/MHz m
β	non-linearity coefficient
δ	acoustic diffusivity
λ	wavelength, m
μ	shear viscosity of blood flow, kg/m s
ρ	density, kg/m ³
Ψ	acoustic velocity potential
ω	angular frequency, MHz

Subscripts

t	tissue
b	blood

acoustic wave and heat sink owing to the perfusion in capillaries [7]. The amount of removed heat can be estimated by averaging the effect of blood perfusion over all tissues. Homogenization assumption is probably no longer valid in modeling the temperature elevation in the regions containing some sufficiently large vessels, inside which the blood is flowing.

Both biologically relevant convective cooling in large blood vessels and perfusion cooling in microvasculatures need to be taken into account altogether. Inclusion of these two possible cooling means will greatly increase the modeling complexity since the equations of motion for the blood flow need to be solved together with the divergence-free velocity constraint equation. Curra et al. [8] developed a model to determine the influence of blood flow on the temperature distribution in the tissue during the focused ultrasound surgery. Their model was constructed on the basis of acoustic and bioheat equations. The blood vessel was on the acoustic axis. Kolios et al. [9] and Hariharan et al. [10] studied the influence of large blood vessels on the lesion size. They considered also only the acoustic equation and bioheat equation. However for a real blood vessel it is necessary to take into account the blood flow motion governed by the non-linear hemodynamic equations. The 3D mathematical acoustics-thermal-fluid model presented in [11] takes the additional acoustic streaming effect into account with an aim to show that the incident finite-amplitude ultrasound wave can affect the blood flow motion in large hepatic vessels and consequently the temperature distribution in tumor. In [11] the numerical simulation was carried out in a patient specific liver geometry. The distance between the focal point and blood vessel was about 1 cm. It was shown that acoustic streaming can affect the blood flow distribution in hepatic arterial branches and lead to a mass flux redistribution. In the present work the simple geometry is considered to understand the effect of acoustic streaming on the temperature distribution. The blood vessel is parallel to the acoustic axis. So far no numerical result, which is computed from the heat transfer equation for large blood vessel and its surrounding tissue coupled with the non-linear hemodynamic equations with an acoustic streaming effect being considered, is ever reported for HIFU tumor ablation. The whole physics remains nowadays poorly understood.

2. Three-field coupling model

Intense ultrasound energy can be delivered to a small region of the targeted tissue. Absorption of energy of this sort in such area

can, as a result, elevate tissue temperature to a certain high magnitude. Such a short-duration temperature increase can destroy tumoral cells with a high dividing rate, thus becoming more sensitive. For the sake of quantifying tissue response to an applied ultrasound, the biological structure in the region under current investigation needs to be taken into account.

2.1. Acoustic equation for ultrasound propagation

The linear Westervelt wave equation [12] given below for ultrasound pressure p will be employed to model the finite-amplitude wave propagation in a soft tissue:

$$\nabla^2 p - \frac{1}{c_0^2} \frac{\partial^2 p}{\partial t^2} + \frac{\delta}{c_0^4} \frac{\partial^3 p}{\partial t^3} + \frac{\beta}{\rho_0 c_0^4} \frac{\partial^2 p^2}{\partial t^2} = 0 \quad (1)$$

The first two terms govern the linear lossless wave propagating at a small-signal sound speed. The third term needs to be included in the current analysis due to thermal conductivity and fluid viscosity. In soft tissues, which are assumed to be thermoviscous, the acoustic diffusivity δ accounts for the thermal and viscous losses in a fluid and is modeled by

$$\delta = \frac{2c_0^3 \alpha}{\omega^2} \quad (2)$$

In the above, α denotes the acoustic absorption coefficient and $\omega (\equiv 2\pi f)$ is the angular frequency. In the current HIFU numerical study, we neglect the non-linear effect, which will be the focus of our future study, for simplifying the analysis.

In this study each small element dS of the transducer surface is assumed to vibrate continuously at the same velocity $u = u_0 \exp(i\omega t)$ along the direction normal to the surface. The resulting linear wave equation can be transformed to the diffraction integral equation for the velocity potential as follows [13,14]

$$\psi_{\bar{p}} = \int \int_S \frac{u}{2\pi r} \exp^{-(\alpha+ik)r} dS \quad (3)$$

In the above, r is the distance from the source point on the transducer surface dS to a field point \bar{p} , and k is the wave number. The pressure amplitude at point \bar{p} can be calculated from the following expression

$$p_{\bar{p}} = ikc\rho_t\psi \quad (4)$$

where ρ_t is the density of tissue, and c is the speed of ultrasound in tissues.

The ultrasound power deposition per unit volume is assumed to be proportional to the local acoustic intensity I as follows

$$q = 2\alpha I \quad (5)$$

The intensity I shown above is defined as

$$I = \frac{p_p^2}{2\rho_t c} \quad (6)$$

Note that Eqs. (3) and (4) consider only the effects of diffraction and attenuation without taking the effect of non-linearity into account. Several studies [8,10,15–18] showed that for a focal intensity in the range of 100–1000 W/cm² and the peak negative pressure in the range of 1–4 MPa, physical complexities such as the cavitation and the highly non-linear wave propagation can be neglected with acceptable errors. In the present study the acoustic energy emitted from the transducer is 80 Watt. The intensity generated at the focus is 280 W/cm² and the pressure at the focal point is 3 MPa. Therefore we do not consider here the effects of non-linearity and cavitation.

Absorption and attenuation coefficients in tissues are normally increased with the ultrasound frequency in a power law form for most media [19]. This is the main reason for the increasing use of high-intensity ultrasound in tissue heating. The penetration depth of ultrasound is, on the other hand, limited by the frequency in accordance with Eq. (3). In this study the transducer with frequency 1.33 MHz is considered. The transducer has a full-width half pressure maximum of ≈ 1.6 mm, which can be considered as an estimation of the lesion width [20].

2.2. Energy equation for tissue heating

Whereas hepatic arteries and portal veins may irrigate the liver parenchyma, hepatic veins will drain blood out of the liver and can, thus, be considered as a heat sink. Tumor cells in perivascular region, as a result, may escape from an externally imposed high heat, leading possibly to a local recurrence. This is one of the major thermal equilibrium processes that takes place in the pre- or post-capillary vessel. Therefore, the mathematical model appropriate for predicting the temperature in tissues must take the heat conduction, tissue perfusion, convective blood cooling, and heat deposition due to an incident wave into account. In this paper we will develop a biologically relevant thermal model by dividing the region of current interest into the region with tissue perfusion, which is due mainly to the capillary beds, and the capillary region containing blood vessels. In other words, in the simulation of thermal field the physical domain has been split into the domains for the perfused tissue and the flowing blood.

In a region free of large blood vessels, the diffusion-type Pennes bioheat equation [7] given below will be employed to model the transfer of heat in the perfused tissue region:

$$\rho_t c_t \frac{\partial T}{\partial t} = k_t \nabla^2 T - w_b c_b (T - T_\infty) + q \quad (7)$$

In the above energy equation proposed for modeling the time-varying temperature in the tissue domain, ρ , c , k denote the density, specific heat, and thermal conductivity, respectively, with the subscripts t and b referring to the tissue and blood domains. The notation T_∞ is denoted as the temperature at a remote location. The variable $w_b (\equiv 0.5 \text{ kg/m}^3 \text{ s})$ shown in Eq. (7) is the perfusion rate for the tissue cooling in capillary flows. It is noted that the above energy equation for T is coupled with the linear acoustic Eq. (4) for the acoustic pressure through a power deposition term q defined in Eq. (5).

In the region containing large vessels, within which the blood flow can convect heat, the biologically relevant heat source, which

is q , and the heat sink, which is $-\rho_b c_b \mathbf{u} \cdot \nabla T$, are added to the conventional diffusion-type heat equation. The resulting energy equation avoids a possible high recurrence stemming from the tumor cell survival next to large vessels

$$\rho_b c_b \frac{\partial T}{\partial t} = k_b \nabla^2 T - \rho_b c_b \mathbf{u} \cdot \nabla T + q \quad (8)$$

In the above, \mathbf{u} is the blood flow velocity. Owing to the presence of blood flow velocity vector \mathbf{u} in the above energy equation, we know that a biologically sound model for conducting a HIFU simulation should comprise a coupled system of thermal-fluid-acoustics non-linear differential equations. In such an analysis framework, the heat sink is coupled with the hydrodynamic equations described later in Section 2.3 and the heat source is governed by the acoustic field equation described previously in Section 2.1.

Thermal dose developed by Sapareto and Dewey [21] will be applied to give us a quantitative relationship between the temperature and time for the tissue heating and the extent of cell killing. In focused ultrasound surgery (generally above 50 °C), the expression for the thermal dose (TD) can be written as:

$$TD = \int_{t_0}^{t_{final}} R^{(T-43)} dt \approx \sum_{t_0}^{t_{final}} R^{(T-43)} \Delta t \quad (9)$$

where $R = 2$ for $T > 43$ °C, $R = 4$ for 37 °C $< T < 43$ °C. The value of TD required for a total necrosis ranges from 25 to 240 min in biological tissues [18,21,22]. According to this relation, thermal dose resulting from heating the tissue to 43 °C for 240 min is equivalent to that achieved by heating it to 56 °C for 1 s.

2.3. Acoustic streaming hydrodynamic equations

Owing to the inclusion of heat sink, which is shown on the right hand side of Eq. (8), the velocity of blood flow plus the velocity resulting from the acoustic streaming due to the applied high-intensity ultrasound must be determined. In this study we consider that the flow in large blood vessels is incompressible and laminar. The vector equation for modeling the blood flow motion, subject to the divergence free equation $\nabla \cdot \mathbf{u} = 0$, in the presence of acoustic stresses is as follows [23,24].

$$\frac{\partial \mathbf{u}}{\partial t} + (\mathbf{u} \cdot \nabla) \mathbf{u} = \frac{\mu}{\rho} \nabla^2 \mathbf{u} - \frac{1}{\rho} \nabla \mathbf{P} + \frac{1}{\rho} \mathbf{F} \quad (10)$$

In the above, \mathbf{P} is the static pressure, μ ($=0.0034 \text{ kg/m s}$) the shear viscosity of blood flow, and ρ the blood density. In Eq. (10), the force vector \mathbf{F} acting on the blood fluid due to ultrasound is assumed to propagate along the acoustic axis \mathbf{n} . The resulting non-zero component in \mathbf{F} takes the following form [25]

$$\mathbf{F} \cdot \mathbf{n} = \frac{2\alpha}{c_0} I \quad (11)$$

The acoustic intensity I shown above has been defined in Eq. (6). Amongst the second-order physical effects, only the acoustic streaming is taken into account in this study.

3. Description of the problem

The HIFU transducer used in this study is a single element, that is spherically focused with an aperture of 12 cm and a focal length of 12 cm. The transducer presumably emits a beam of spherically-shaped ultrasound wave and will propagate towards the targeted tissue under the current investigation. The parameters used in the current simulation are listed in Table 1 [11,26].

We consider the case of a linear dependance of the attenuation coefficient on frequency [26]. In this study, we will consider the transducer with the frequency $f = 1.33$ MHz. The acoustic energy

Table 1
Acoustic and thermal properties for the liver tissue and blood.

Tissue	c_0 ($\frac{m}{s}$)	ρ ($\frac{kg}{m^3}$)	c ($\frac{J}{kgK}$)	k ($\frac{W}{mK}$)	α ($\frac{Np}{m}$)
Liver	1550	1055	3600	0.512	$9 * f$
Blood	1540	1060	3770	0.53	$1.5 * f$

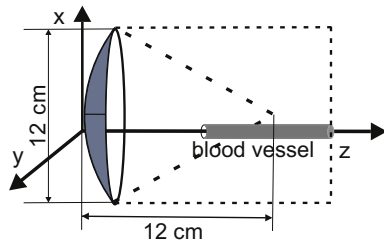


Fig. 1. Schematic of the physical model. Blood vessel is parallel to the acoustic axis. The space bounded by the dashed line and the transducer is the domain for conducting acoustic wave simulation.

emitted from this transducer is 80 Watt. The initial temperature is equal to 37 °C and the blood flow is 0.13 m/s prescribed on the inlet vessel plane [27]. The vessel diameter is 3 mm. We assume a parabolic velocity profile at the inlet of blood vessel. As the duration of energy delivery ranges from 5 to 12 s [28], the solid tumor was assumed to be exposed to a 8 s ultrasound. The blood vessel schematic in Fig. 1 is parallel to the acoustic axis. The distance between the blood vessel wall and focal point ranges from 1.0 mm to 0.5 mm.

The three-dimensional problem is analyzed using the commercially available CFDRC (CFDRC Research, Hunstille, AL, USA) software. A detailed description of the solution procedures can be found in our previous article [11]. For the calculation of the temperature and velocity fields we used the computational domain with dimensions 6 cm × 4 cm × 4 cm. It is sufficient for the considered treatment time. In the focal region (4 mm × 4 mm × 20 mm) the refined grids were generated with a mesh length 0.2 mm. The number of grids used in this study was 126465 in the blood vessel and 525736 in the liver. Mesh independence was assessed by comparing the temperature distribution in the final working mesh with the temperature obtained in a refined mesh, which is generated by increasing the number of cells by 30%. In two meshes, the temperatures differ from each other only by an amount less than 1%.

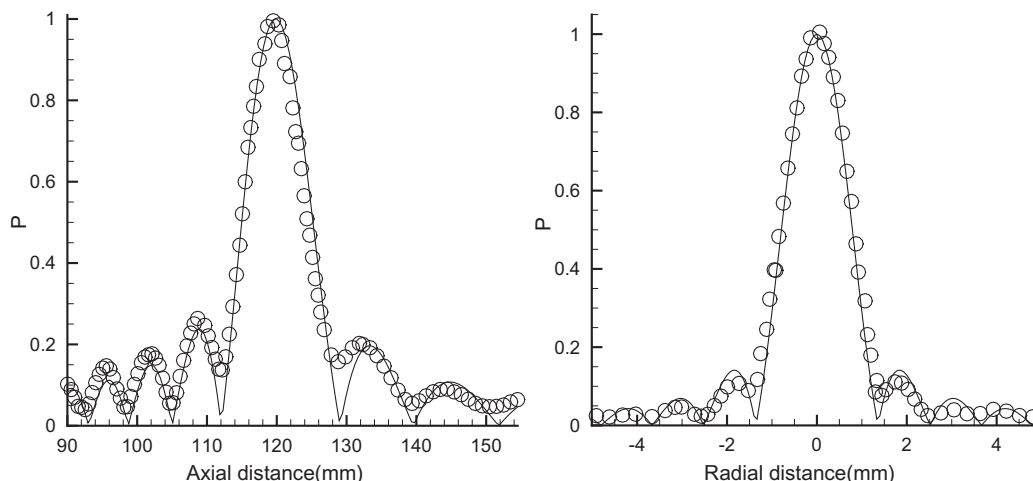


Fig. 2. The measured and computed pressure profiles in water at 1.33 MHz and 1.45 MPa pressure at the focal point.

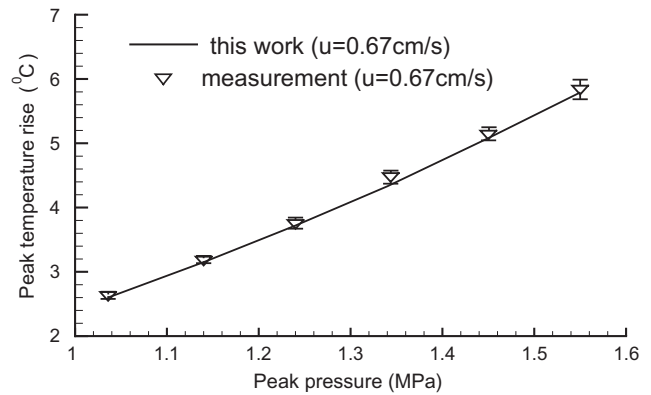


Fig. 3. Comparison of the simulated peak temperature rise at the focus (positioned in a phantom material and 0.4 mm from the vessel wall) with the experimental data [25] as a function of pressure for the flow speed $u = 0.67$ cm/s in the vessel.

4. Comparison with the experimental data

In order to verify our theoretical analysis, the following experiments were carried out. The acoustic source and hydrophone were immersed in a water tank, which was open to the atmosphere. A three-dimensional computerized positioning system was designed to move the transducer along the beam axis and orthogonal directions. The investigated single-element transducer has a focal length of 120 mm, an aperture of 120 mm and frequency of 1.33 MHz. The transducer was driven by a continuous wave. In Fig. 2, the pressure profile is plotted against the radial and axial distances (in the focal plane). Solid lines and open circles correspond to the prediction and measurement results, respectively. These results were obtained in water at 25 °C using the chosen 0.4 mm hydrophone (Onda HNA-0400). The efficiency of the transducer was measured by the radiation force balance. The measured pressures were normalized by the focal pressure of 1.45 MPa. We can see a good agreement between the measured and numerical results. Since power deposition is quadratic in pressure, the deviation between the measurement and model analysis in the low amplitude regions is not deemed significant.

The present computational model was validated by comparing our simulated results with the experimental results of Huang et al. [25]. This comparison was made for the temperature field in a tissue phantom with 2.6 mm blood vessel. The results of comparison are presented in Fig. 3. The acoustic frequency and

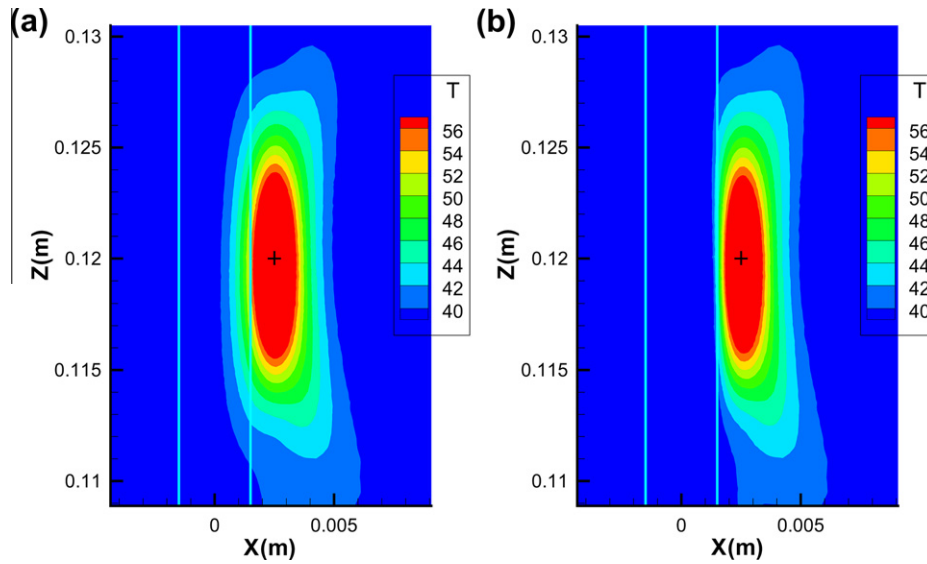


Fig. 4. The predicted temperature contours at $t = 8$ s in liver at the cutting plane $y = 0$ for the case investigated at $f = 1.33$ MHz and 3.0 MPa pressure at the focal point, cross (+) denotes the location of focal point (0.0025,0,0.12). (a) without blood flow; (b) with blood flow, $u = 0.13$ m/s.

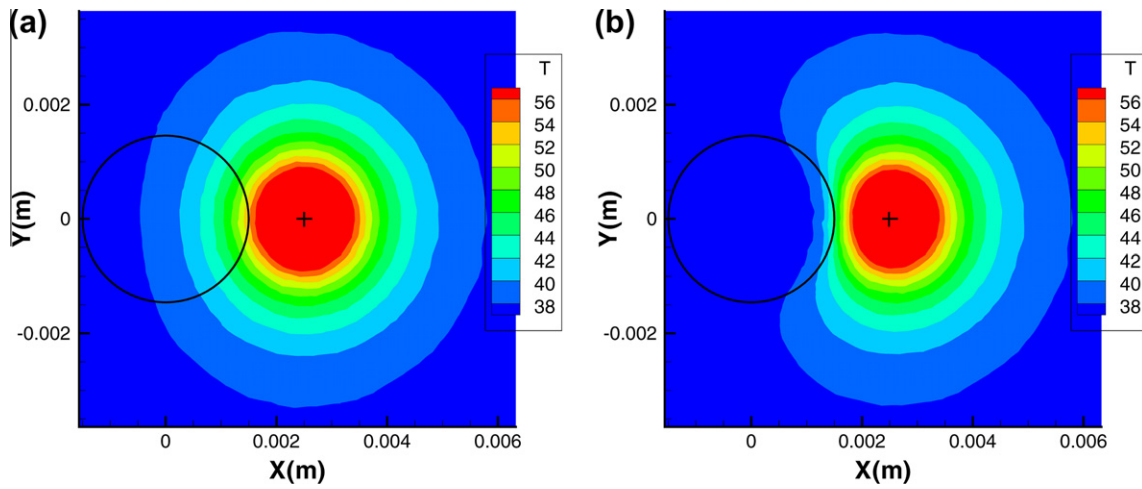


Fig. 5. The predicted temperature contours at $t = 8$ s in liver at the cutting plane $z = 0.12$ m for the case investigated at $f = 1.33$ MHz and 3.0 MPa pressure at the focal point, cross (+) denotes the location of focal point (0.0025,0,0.12). (a) without blood flow; (b) with blood flow, $u = 0.13$ m/s.

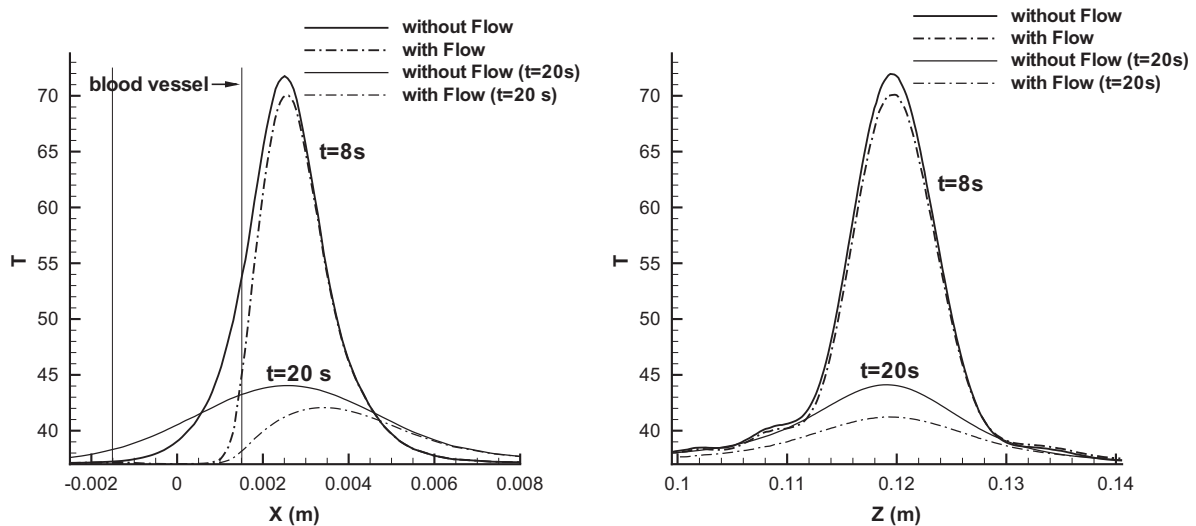


Fig. 6. The predicted temperature distributions along x and z directions at $t = 8$ s (just after sonication) and $t = 20$ s (the transducer is switched off at $t = 8$ s) for the cases with and without blood flow investigated at $f = 1.33$ MHz and focal intensity 280 W/cm².

sonication time were 1.0 MHz and 5 s, respectively. Radius of transducer was 7 cm, and focal length is 6.3 cm. Our results are in a good agreement with the experimental data of Huang et al. [25] for the mean flow velocity of 0.67 cm/s within the estimated uncertainties in temperature measurements.

5. Results and discussion

The proposed three-field coupling mathematical model is used to get the temperature distribution in liver. First we will study the temperature distribution in liver, when the distance between the focal axis and blood vessel is 1 mm. The inlet velocity is set at 0.13 m/s.

In Figs. 4, 5 we can see the computed temperature contours at $t = 8$ s (or s) in the liver at the cutting planes $y = 0$ and $z = 0.12$ m for the cases with and without blood flow. In these figures we do not show the simulated temperature that is higher than 56°C , be-

cause as we mentioned before it is the threshold value for the tissue necrosis. For the case without blood flow an ellipsoidal lesion with the dimension $8.6\text{ mm} \times 1.8\text{ mm} \times 1.8\text{ mm}$ is obtained. The blood flow reduces the lesion size in both axial and radial directions. For the case with flow the lesion size is reduced from 8.6 to 8.0 mm in the axial direction. The distance between the lesion and blood vessel wall is 0.12 mm for the case without flow and is equal to 0.3 mm, when we take into account blood flow motion. This explains why the tissues close to blood vessel remain viable. A layer of tissues close to the blood vessel receives a lower thermal dose due to the blood cooling.

In Fig. 6 we can see the temperature profiles computed at $t = 8$ s and at $t = 20$ s (the transducer is switched off at $t = 8$ s) along the focal axis z and the radial axis x . The peak temperature is 71.8°C at the focus in the absence of blood flow. If we take into account the blood flow, the maximal temperature becomes 70°C . Temperature profile becomes asymmetric in the presence of blood flow.

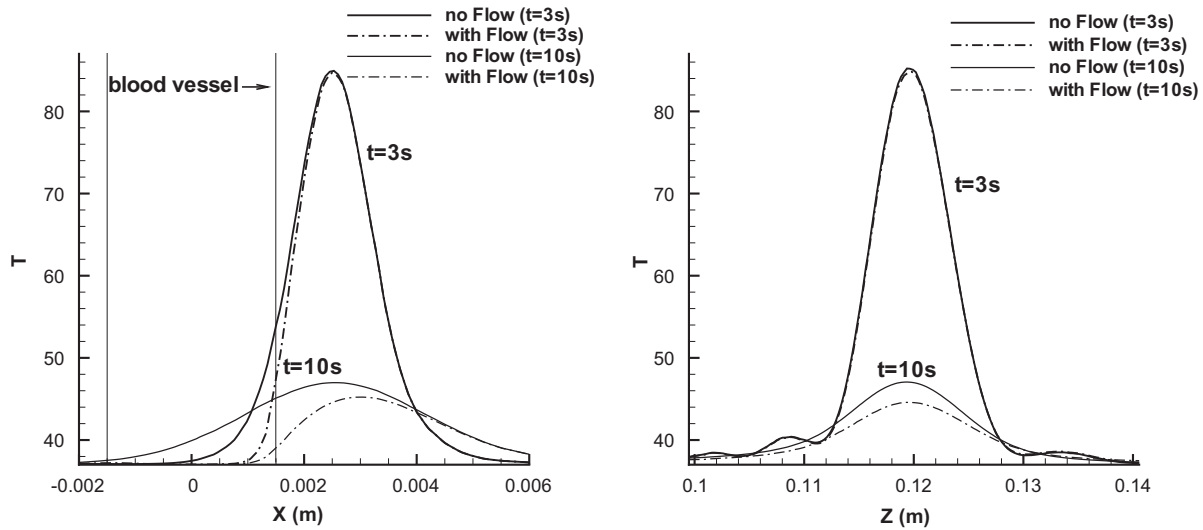


Fig. 7. The predicted temperature distributions along x and z directions at $t = 3$ s (just after sonication) and $t = 10$ s (the transducer is switched off at $t = 3$ s) for the cases with and without blood flow investigated at $f = 1.33$ MHz and focal intensity 600 W/cm^2 .

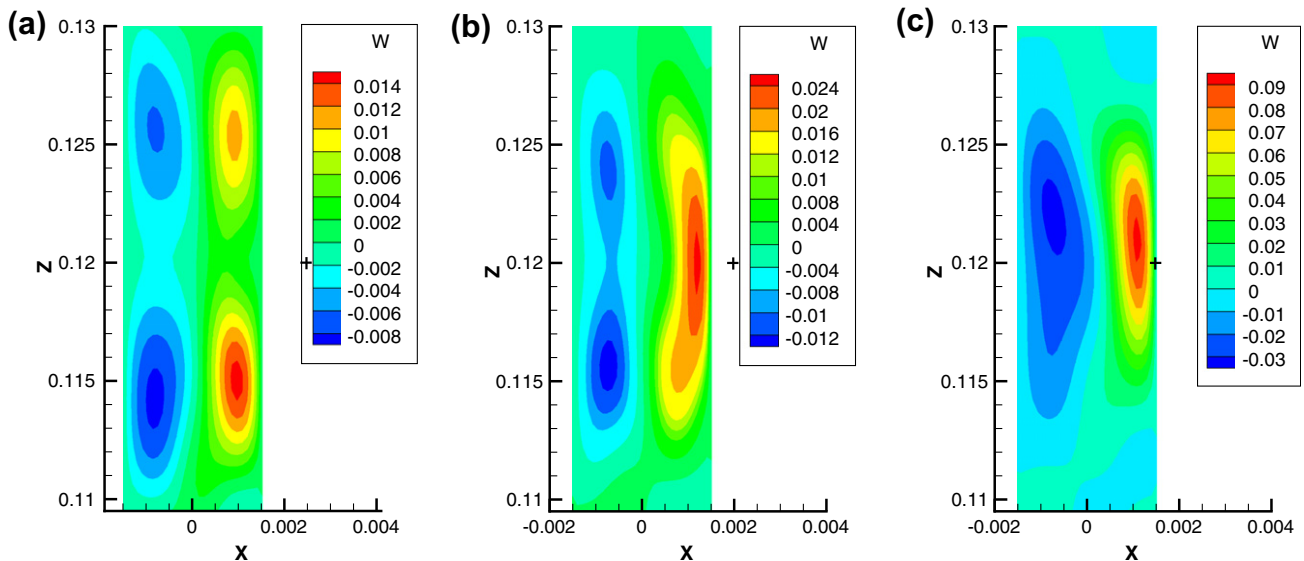


Fig. 8. The simulated streaming profiles at the cutting plane $y = 0$ m without the externally applied flow for different distances between the focal point and the vessel wall. w – velocity in z direction, m/s. (a) focal point is at $x = 0.0025$ m, $z = 0.12$ m, at a distance 1.0 mm from the vessel wall; (b) focal point is at a distance 0.5 mm from the vessel wall; (c) focal point is at $x = 0.0015$ m, on the blood vessel wall.

Table 2

Maximum acoustic streaming velocity U_{max} (m/s) computed in the blood vessel for different distances between the focal point and blood vessel wall.

Intensity, W/ cm ²	U_{max} , gap = 1 mm	U_{max} , gap = 0.5 mm	U_{max} , gap = 0 mm
280	0.014	0.026	0.09
600	0.025	0.05	0.17

There is a very fast temperature decrease near the blood vessel wall. The maximal temperature along the radial axis shifts 0.1 mm from the focal point at $t = 8$ s. At $t = 20$ s the peak temperature at the focal point is 44.1 °C for the case without blood flow and 42.1 °C for the case with blood flow. At $t = 20$ s, in the presence of blood flow the peak temperature shifts 0.9 mm from the focal point along the radial axis. At time $t = 20$ s there is a large difference between the temperature distributions for the cases with and without blood flow. We have computed the temperature for

several distances between the focal point and blood vessel wall. The calculated results show that large blood vessel can significantly change the temperature distribution in liver tumor when the distance between the focal point and blood vessel wall is equal to several mm. In Fig. 7 the temperature profiles are presented for an exposure time $t = 3$ s and focal intensity 600 W/cm². At time $t = 3$ s the temperature difference at the focal point (1 mm from the vessel wall) is less than 1% for the cases considered with and without flow. The effect of blood flow cooling decreases with the decreased treatment time. Next we will study the effect of acoustic streaming on the velocity and temperature distributions in the investigated domain.

In Fig. 8 we present the z velocity component at the cutting plane $y = 0$ for different gaps. Note that the gap schematic in Fig. 1 is the distance between the focal point and the vessel wall. We consider initially the steady-state flow. Acoustic streaming velocity is induced by the absorbed ultrasound energy. When the gap is equal to 0 mm, one large eddy circulation appears. For the

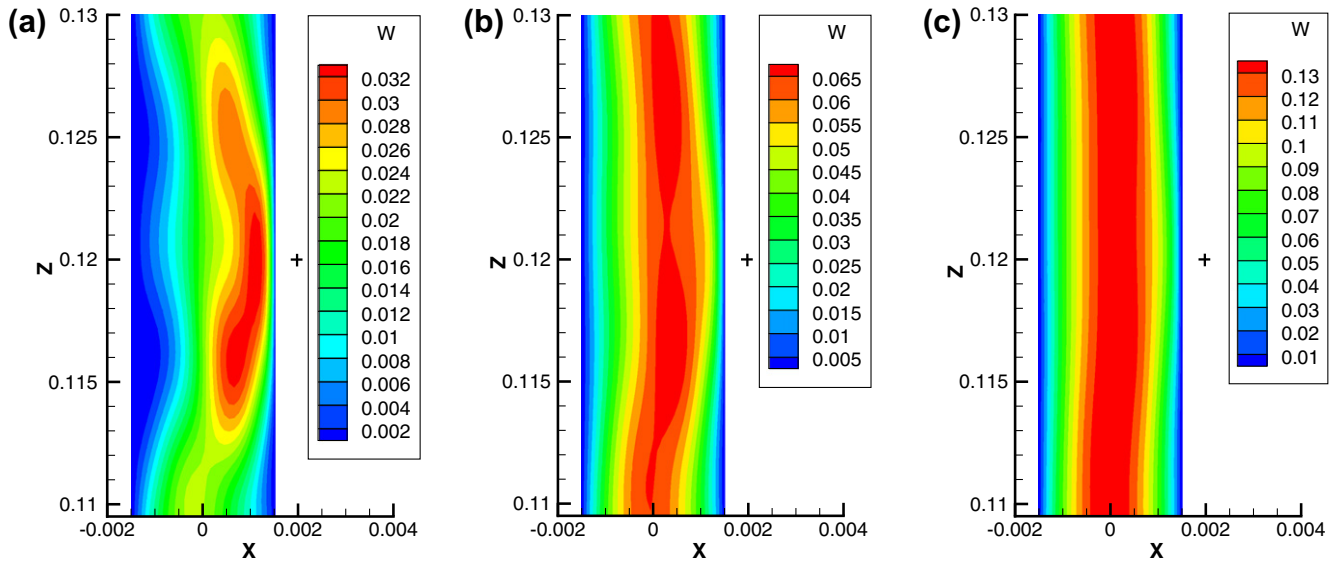


Fig. 9. The predicted acoustic streaming velocity profiles at the cutting plane $y = 0$ for different initial velocities. Focal point (0.002,0.0.12) is 0.5 mm from the vessel wall. (a) blood flow velocity $u = 0.02$ m/s; (b) velocity = 0.06 m/s; (c) velocity = 0.13 m/s.

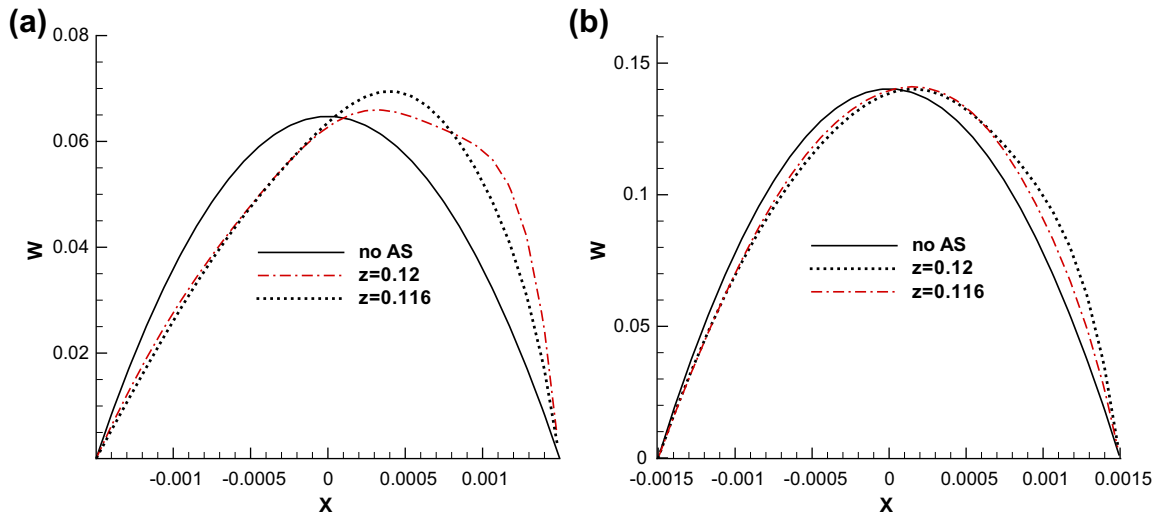


Fig. 10. The simulated velocity profiles $w(x, y = 0, z)$ at three chosen cross-sections z for the cases with and without acoustic streaming. Focal point is 0.5 mm from the vessel wall: (a) blood flow velocity is 0.06 m/s; (b) blood flow velocity is 0.13 m/s.

case with a larger gap (1.0 mm or 0.5 mm), two eddies appear near the focal region in the blood vessel. The maximum acoustic streaming velocity in blood vessel induced by the absorbed ultrasound energy ranges from 0.014 m/s, when the gap is 1.0 mm, to 0.09 m/s, when the gap is 0 mm (when the focal point is on the blood vessel wall). The velocity gradients associated with the acoustic streaming motion are very high, especially, near the boundaries. If we increase the focal intensity from 280 W/cm² to 600 W/cm², the acoustic streaming flow behavior will not change, but the velocity magnitude will change. The comparison of streaming velocity magnitudes for focal intensities 280 W/cm² and 600 W/cm² is presented in Table 2. The maximum acoustic streaming velocity will be 0.025 m/s (0.014 m/s for 280 W/cm²), when the gap is 1.0 mm, and 0.17 m/s (0.09 m/s for 280 W/cm²), when the gap is 0 mm. Increase of focal intensity from 280 W/cm² to 600 W/cm² causes an increase of acoustic streaming velocity magnitude almost twice. In Fig. 9 we can see how the acoustic streaming can alter the blood flow velocity. Initially we consider a parabolic velocity profile in the blood vessel with a maximal velocity $u = 0.02$ m/s, 0.06 m/s and 0.13 m/s. The absorbed ultrasound

energy can increase the maximum velocity (0.032 m/s) near the focal point by 1.6 times of the initial velocity 0.02 m/s. In Fig. 10 the simulated velocity profiles at three chosen cross-sections are presented for the cases with and without acoustic streaming for the blood flow velocities investigated at 0.06 m/s and 0.13 m/s. When we take into account the acoustic streaming effect, blood flow becomes asymmetric. If we increase the initial velocity, the importance of acoustic streaming will decrease. For the presented cases we get a larger velocity gradient near the blood vessel boundary, when we take into account the acoustic streaming effect. This will increase the blood flow cooling.

The predicted temperature distributions at different points along the radial axis are presented in Fig. 11 as function of time for an 8 s sonication for the cases investigated with and without inclusion of acoustic streaming. The imposed velocities are equal to 0.02 m/s, 0.04 m/s and 0.13 m/s. The distance between the focal point and the blood vessel wall (the gap) is equal to 0.5 mm. The largest difference for all cases can be seen at the end of the sonication, $t = 8$ s. On the blood vessel wall (Fig. 11c) at $t = 8$ s the temperature rise is 18.5 °C without the acoustic streaming effect and

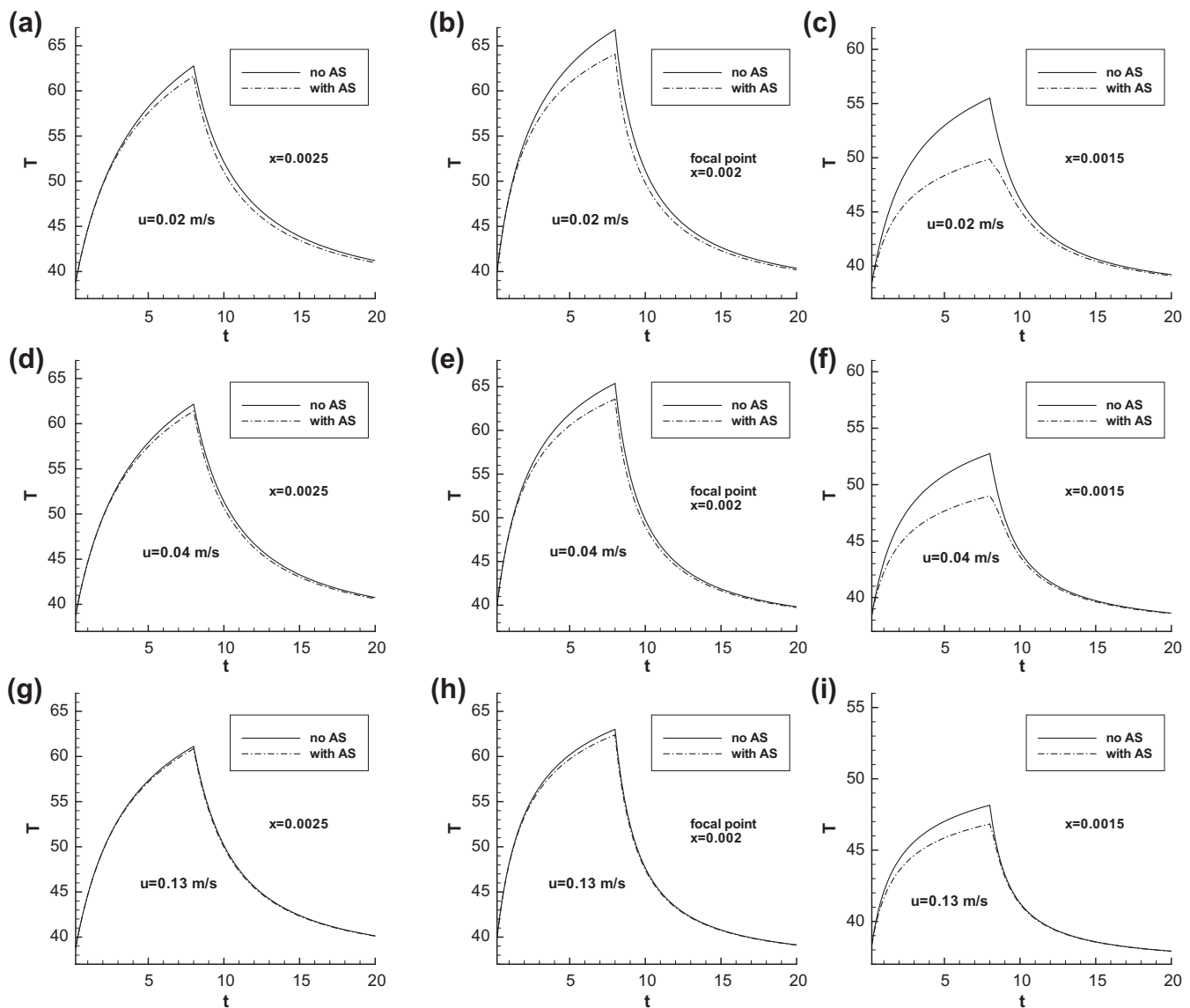


Fig. 11. The predicted temperatures versus time at different radial axis points ($x, y = 0, z = 0.12$) for the cases with and without acoustic streaming for different values of blood flow velocities u : (a) $x = 0.0025$ m, $u = 0.02$ m/s; (b) $x = 0.002$ m (at the focal point), $u = 0.02$ m/s; (c) $x = 0.0015$ m, at the blood vessel wall, $u = 0.02$ m/s; (d) $x = 0.0025$ m; (e) $x = 0.002$ m, $u = 0.04$ m/s; (f) $x = 0.0015$ m, $u = 0.04$ m/s; (g) $x = 0.0025$ m, $u = 0.13$ m/s; (h) $x = 0.002$ m, $u = 0.13$ m/s; (i) $x = 0.0015$ m, $u = 0.13$ m/s.

12.9 °C with the acoustic streaming effect. This means that the temperature rise was reduced by 30% due to the acoustic streaming effect. At the distance 1 mm from the vessel wall (Fig. 11a) the highest temperatures are equal respectively to 62.7 °C and 61.6 °C for the cases considered with and without acoustic streaming correspondingly. Even for a high value of imposed velocity 0.13 m/s we can observe that acoustic streaming can increase blood flow cooling and decrease the temperature significantly. The effect of acoustic streaming is more pronounced for small blood velocities. For the case with a smaller distance between the blood vessel wall and focal point, the effect of the acoustic streaming will increase.

In Fig. 12 we present the predicted lesion boundaries in liver for the cases with and without acoustic streaming effect for the focal intensity 280 W/cm² and sonication time 8 s. The distance between the focal point and the blood vessel wall (the gap) is equal to 0.5 mm, blood flow velocity is 0.02 m/s. When taking into account the acoustic streaming effect, the lesion size can be significantly reduced by 23%. The distance between the vessel wall and

lesion boundary increases from 0.03 mm to 0.16 mm, when we take into account acoustic streaming effect. It means that acoustic streaming effect cannot be neglected in the treatment planning. When the distance between the focal point and the blood vessel boundary becomes smaller, the effect of acoustic streaming will be more pronounced. In Fig. 13 we present the predicted lesion boundaries in liver for the cases with and without acoustic streaming effect for the larger value of focal intensity 600 W/cm² and smaller sonication time 3 s. When taking into account the acoustic streaming effect, the lesion size is reduced by 16%. Even for small sonication time (3 s) acoustic streaming effect can affect the lesion size. The distance between the vessel wall and lesion boundary is 0.03 mm (the distance was 0.16 mm for the focal intensity 280 W/cm² and sonication time 8 s). Higher focal intensities and shorter sonication times can significantly reduce the distance between the lesion boundary and blood vessel wall. If destruction of all cells near the blood vessel boundary is necessary, a shorter sonication time with higher power deposition is suggested so as to minimize the viable region.

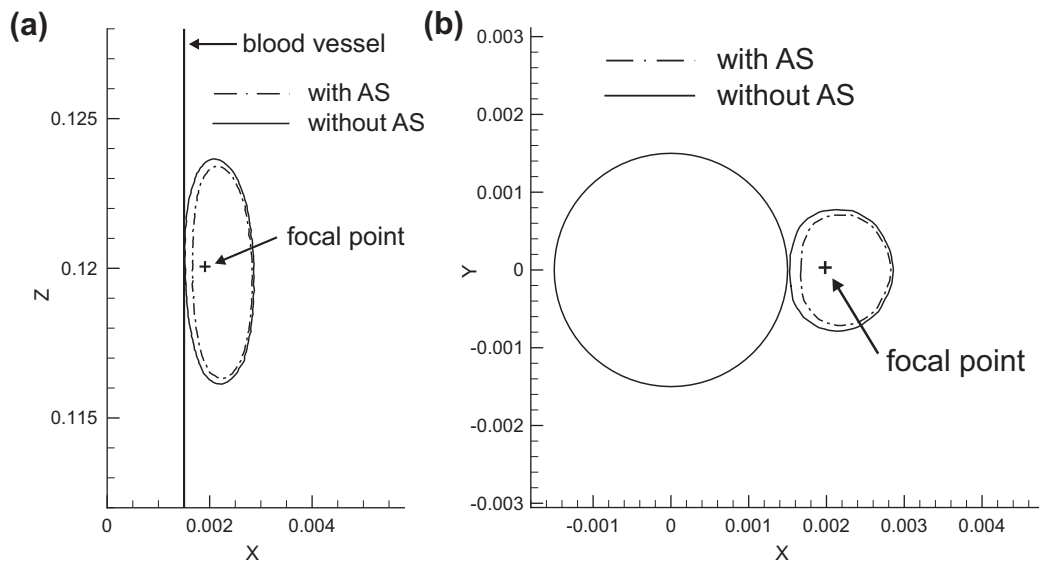


Fig. 12. The predicted lesion shapes in liver for the cases with and without acoustic streaming effect, gap = 0.5 mm, focal intensity = 280 W/cm², sonication time 8 s, and blood flow velocity is 0.02 m/s. (a) at the cutting plane $y = 0$; (b) at the cutting plane $z = 0.12$ m.

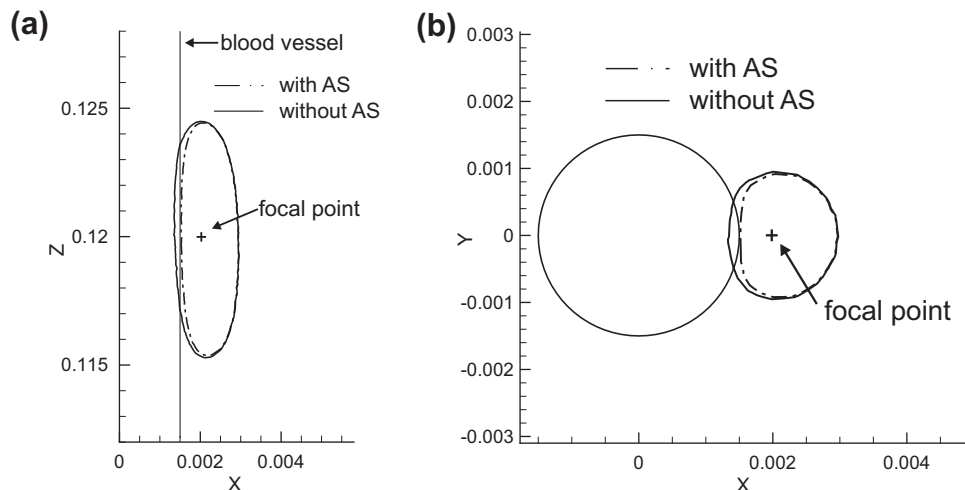


Fig. 13. The predicted lesion shapes in liver for the cases with and without acoustic streaming effect, gap = 0.5 mm, focal intensity = 600 W/cm², sonication time 3 s, and blood flow velocity is 0.02 m/s. (a) at the cutting plane $y = 0$; (b) at the cutting plane $z = 0.12$ m.

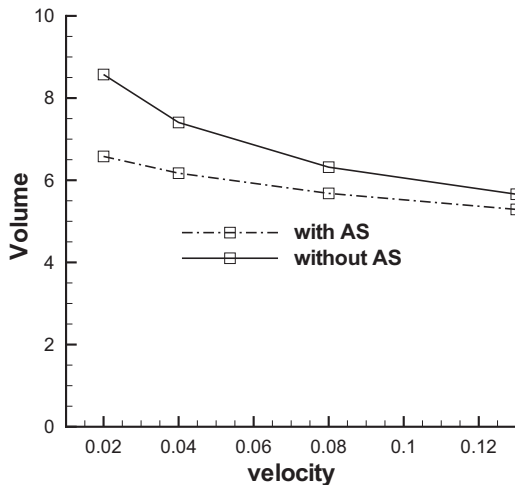


Fig. 14. The simulated ablated tumor volumes (mm^3) as the function of initial velocity (m/s) for the cases with and without acoustic streaming.

The simulated ablated tumor volumes, which vary with the initial velocity, for the cases with and without flow are presented in Fig. 14. The distance between the blood vessel boundary and focal point is 0.5 mm. When we increase the velocity from 0.02 m/s to 0.04 m/s, the volume calculated without taking into account the acoustic streaming effect is changed by an amount of 14%. When we increase the velocity from 0.08 m/s to 0.13 m/s, the difference of the volumes is only about 10%. A further increase of the velocity will decrease the ablated volume by only a small value. This means that inclusion of acoustic streaming into analysis decreases the ablated tumor volume. At the velocity 0.02 m/s the difference of volumes for the cases considered with and without acoustic streaming is equal to 23%. With the increasing initial velocity the difference will decrease. For the case with the velocity 0.13 m/s the difference of volumes is only 7%.

6. Conclusion

We have proposed a three dimensional physical model to conduct the current HIFU study. The proposed model takes into account the convective cooling in large blood vessel and the perfusion due to capillary flows. Convective cooling in large blood vessel was shown to reduce the temperature near a large blood vessel. Acoustic streaming was also included in the simulation model. Due to the cooling effect enhanced by acoustic streaming, the temperature rise near the blood vessel wall is much lower than the value predicted without taking into account the acoustic streaming effect. It was shown that acoustic streaming generated by ultrasound can affect the lesion size and the shape. This demonstrates the necessity of taking into account both of the convective cooling and acoustic streaming effects for a simulation involving a large blood vessel, when the tumor is close to large blood vessel.

Acknowledgment

The authors would like to acknowledge the financial support from the National Science Council under the Projects NSC 99-2628-M-002-005 and NSC 97-2221-E-002-250-MY3.

References

- [1] M. Thiriet, *Biology and Mechanics of Blood Flows. Part II: Mechanics and Medical Aspects*, Springer, New York, 2008.
- [2] Y.F. Zhou, High intensity focused ultrasound in clinical tumor ablation, *World J. Clin. Oncol.* 2 (1) (2011) 8–27.
- [3] T.A. Leslie, J.E. Kennedy, High intensity focused ultrasound in the treatment of abdominal and gynaecological diseases, *Int. J. Hyperther.* 23 (2007) 173–182.
- [4] F. Wu, Z.B. Wang, W.Z. Chen, H. Zhu, J. Bai, J.Z. Zou, K.Q. Li, C.B. Jin, F.L. Xie, H.B. Su, Extracorporeal high intensity focused ultrasound ablation in the treatment of patients with large hepato cellular carcinoma, *Ann. Surg. Oncol.* 11 (2004) 1061–1069.
- [5] R.O. Iling, J.E. Kennedy, F. Wu, G.R. ter Haar, A.S. Protheroe, P.J. Friend, F.V. Gleeson, D.W. Cranston, R.R. Phillips, M.R. Middleton, The safety and feasibility of extracorporeal high-intensity focused ultrasound (HIFU) for the treatment of liver and kidney tumours in a western population, *Br. J. Cancer* 93 (2005) 890–895.
- [6] L. Zhang, H. Zhu, C. Jin, K. Zhou, K. Li, H. Su, W. Chen, J. Bai, Z. Wang, High-intensity focused ultrasound (HIFU): effective and safe therapy for hepatocellular carcinoma adjacent to major hepatic veins, *Eur. Radiol.* 19 (2009) 437–445.
- [7] H.H. Pennes, Analysis of tissue and arterial blood temperature in the resting human forearm, *J. Appl. Physiol.* 1 (2) (1948) 93–122.
- [8] F.P. Curra, P.D. Mourad, V.A. Khokhlova, R.O. Cleveland, L.A. Crum, Numerical simulations of heating patterns and tissue temperature response due to high-intensity focused ultrasound, *IEEE Trans. Ultrason. Ferroelectr. Freq. Control* 47 (2000) 1077–1089.
- [9] M.C. Kolios, M.D. Sherar, J.W. Hunt, Large blood vessel cooling in heated tissues: a numerical study, *Phys. Med. Biol.* 40 (1995) 477–494.
- [10] P. Hariharan, M.R. Myers, R.K. Banerjee, HIFU procedures at moderate intensities – effect of large blood vessels, *Phys. Med. Biol.* 52 (12) (2007) 3493–3513.
- [11] T.W.H. Sheu, M.A. Solovchuk, A.W.J. Chen, M. Thiriet, On an acoustics-thermal-fluid coupling model for the prediction of temperature elevation in liver tumor, *Int. J. Heat Mass Transfer* 54 (17–18) (2011) 4117–4126.
- [12] M.F. Hamilton, D.T. Blackstock, *Nonlinear Acoustics*, Academic Press, Boston, 1998.
- [13] A.D. Pierce, *Acoustics: An Introduction to its Physical Principles and Applications*, McGraw-Hill, New York, 1981.
- [14] H.T. O'Neil, Theory of focusing radiators, *J. Acoust. Soc. Am.* 21 (5) (1949) 516–526.
- [15] M. Bailey, V. Khokhlova, O. Sapozhnikov, S. Kargl, L. Crum, Physical mechanism of the therapeutic effect of ultrasound (a review), *Acoust. Phys.* 49 (4) (2003) 369–388.
- [16] I. Hallaj, R. Cleveland, FDTD simulation of finite-amplitude pressure and temperature fields for biomedical ultrasound, *J. Acoust. Soc. Am.* 105 (5) (1999) L7–L12.
- [17] E.A. Filonenko, V.A. Khokhlova, Effect of acoustic nonlinearity on heating of biological tissue by high-intensity focused ultrasound, *Acoust. Phys.* 47 (4) (2001) 468–475.
- [18] P.M. Meaney, M.D. Cahill, G.R. ter Haar, The intensity dependence of lesion position shift during focused ultrasound surgery, *Ultrasound Med. Biol.* 26 (3) (2000) 441–450.
- [19] C.R. Hill, J.C. Bamber, G.R. Haar, *Physical Principles of Medical Ultrasonics*, John Wiley and Sons, 2004.
- [20] C.R. Hill, I. Rivens, M.G. Vaughan, G.R. Ter Haar, Lesion development in focused ultrasound surgery: a general model, *Ultrasound Med. Biol.* 20 (3) (1994) 259–269.
- [21] S.A. Sapareto, W.C. Dewey, Thermal dose determination in cancer therapy, *Int. J. Radiat. Oncol. Biol. Phys.* 10 (6) (1984) 787–800.
- [22] H.L. Liu, H. Chang, W.S. Chen, T.C. Shih, J.K. Hsiao, W.L. Lin, Feasibility of transrib focused ultrasound thermal ablation for liver tumors using a spherically curved 2D array: a numerical study, *Med. Phys.* 34 (9) (2007) 3436–3448.
- [23] T. Kamakura, M. Matsuda, Y. Kumamoto, M.A. Breazeale, Acoustic streaming induced in focused Gaussian beams, *J. Acoust. Soc. Am.* 97 (1995) 2740–2746.
- [24] K. Matsuda, T. Kamakura, Y. Kumamoto, Build up of acoustic streaming in focused beams, *Ultrasonics* 34 (1996) 763–765.
- [25] J. Huang, R.G. Holt, R.O. Cleveland, R.A. Roy, Experimental validation of a tractable medical model for focused ultrasound heating in flow-through tissue phantoms, *J. Acoust. Soc. Am.* 116 (4) (2004) 2451–2458.
- [26] F.A. Duck, *Physical Property of Tissues – A Comprehensive Reference Book*, Academic, London, 1990.
- [27] F.A. Duck, A.C. Baker, H.C. Starrit, *Ultrasound in Medicine*, Institute of Physics Publishing, Bristol, 1998.
- [28] K. Fischer, W. Gedroyc, F. Jolesz, Focused ultrasound as a local therapy for liver cancer, *Cancer J.* 16 (2) (2010) 118–124.